Determination of the effective diffusion length of silicon solar cells from photoluminescence

David Hinken,[a] Karsten Bothe, Klaus Ramspeck, Sandra Herlufsen, and Rolf Brendel
Institut für Solarenergieforschung Hameln (ISFH), Am Ohrberg 1, 31860 Emmerthal, Germany

(Received 14 January 2009; accepted 12 April 2009; published online 28 May 2009)

We present a method to determine the effective diffusion length L_{eff} of silicon solar cells from photoluminescence (PL) measurements carried out under two different operating conditions. Measuring the photoluminescence emission under open circuit condition (PL-oc), where the solar cell is not contacted at all, and short circuit condition (PL-sc), where the solar cell is held at zero voltage, L_{eff} directly follows from the ratio of the PL-oc and the PL-sc signals. Detailed knowledge about the optical properties of the experimental setup is not necessary since the optical properties cancel out completely. We explain the theoretical background of our method and derive an analytical description for the PL-oc and the PL-sc luminescence emissions. The applicability of our method is demonstrated by the comparison of effective diffusion lengths from PL measurements with values determined from the analysis of internal quantum efficiency measurements. © *2009 American Institute of Physics*. [DOI: 10.1063/1.3130408]

I. INTRODUCTION

The effective diffusion length L_{eff} of minority carriers in the solar cell base is one of the most important parameters when analyzing charge collection properties of silicon solar cells. L_{eff} is defined by the bulk diffusion length L, the device thickness W, and the rear surface recombination velocity S_r.[1] The general approach to determine L_{eff} is to generate different minority carrier distributions in the base of the solar cell meanwhile measuring the impact on a certain solar cell quantity.

One of the most widely used approaches to determine L_{eff} is based on the analysis of the internal quantum efficiency (IQE).[1] For this method, the solar cell is illuminated with monochromatic light of different wavelengths meanwhile its short circuit current is measured. Depending on the illuminated area, the IQE analysis provides global[1] or spatially resolved information as in the case of spectrally resolved light beam induced current (SR-LBIC).[2] Even though the IQE analysis allows for an accurate determination of L_{eff}, a major drawback of this method is that it requires exact information on the reflection properties of the solar cell as well as an accurate calibration of the incident photon flux. Alternatively, as has been demonstrated by Taretto *et al.*,[3] L_{eff} might also be extracted from *I-V* measurements having additional knowledge on the base doping concentration of the solar cell under test.

The analysis of the luminescence emission[4–6] of silicon solar cells might also allow for an accurate determination of L_{eff} since the luminescence emission is related to the carrier distribution within the solar cell base. First experimental evidence that the electroluminesence (EL) emission measured using a charge coupled device camera is closely related to the effective diffusion length was given by Fuyuki *et al.*[7] Further investigations were carried out by Würfel *et al.*[8] who introduced an approach to extract the bulk diffusion length L utilizing the reabsorption of luminescence photons. Since short wavelength luminescence photons have a higher reabsorption probability the restriction of the luminescence spectrum contributing to the EL signal by different optical filters allows to gain a depth information of the carrier distribution within the solar cell base. The physics behind this approach has been further explored by Kirchartz *et al.*,[9] who pointed out the link between the EL emission and the external quantum efficiency (EQE), which are connected by a reciprocity theorem introduced by Rau.[10] Even though these approaches are very elegant with respect to basic physics, detailed information about the experimental setup, like the exact quantum efficiency of the detector as well as the transmission curves of the filters are required.

In this contribution, we introduce an approach to determine the effective diffusion length L_{eff} based on the analysis of the photoluminescence (PL) signal obtained under two different electrical operating conditions. Measuring the luminescence emission under open circuit (PL-oc) and under short circuit condition (PL-sc), L_{eff} directly follows from the ratio of the PL-oc and the PL-sc signals. We explain the theoretical background and present a simple analytical equation describing these two conditions. The advantage of our approach is that no calibration and no detailed informations about the setup are required since optical effects cancel out completely. In the following, we refer to this method as PL-L_{eff}, which is, in general, applicable to spot as well as to spatially resolved measurements using a camera.[11] We demonstrate the applicability of this method by comparing our results to global L_{eff} values determined by the analysis of IQE data.

II. THEORY

The radiative recombination of an electron and a hole results in the emission of a luminescence photon. Thus, the generation rate of the luminescence photons G_{ph} equals the rate of radiative recombination R_{rad},

[a]Electronic mail: hinken@isfh.de.

$$G_{\mathrm{ph}} = R_{\mathrm{rad}} = B_{\mathrm{rad}} np. \tag{1}$$

where B_{rad} is the coefficient of radiative recombination and n and p are the electron and hole densities.

To describe the local luminescence emission Φ of one point of the solar cell surface, we have to integrate G_{ph} over the depth z of the solar cell

$$\Phi = \int dz\, \eta B_{\mathrm{rad}} np. \tag{2}$$

Here, η is an escape probability factor accounting for the reabsorption of the luminescence photons and for reflections at the front and rear surface. In general, η is a function of z because a photon traveling a specific distance through the semiconductor has a certain probability to be reabsorbed.[12] However, the probability for reabsorption decreases for increasing wavelength. Restricting the analysis to wavelength above 1100 nm, $\eta(z)$ only varies by 1% with z for a 200 μm thick silicon sample with Lambertian surfaces and a rear reflection of 100%. Thus, the impact of reabsorption becomes negligible and we take η out of the integral.

Our calculations are carried out for a one-dimensional device structure. Without loss of generality we assume a p-doped base region of thickness W and an n-doped emitter at the front side. The contribution of a thin emitter to the total luminescence emission is negligible,[13] allowing us to restrict the integral in Eq. (2) to the base region of the device. For low-level injection, the product of electron and hole carrier densities, $n(z)\cdot p(z)$, equals in good approximation the product of the excess carrier density $\Delta n(z)$ and the base doping concentration N_A. Moreover B_{rad} is assumed to be independent of z,[14] simplifying Eq. (2) to

$$\Phi = \eta N_A B_{\mathrm{rad}} \int_0^W dz \Delta n(z) = \eta N_A B_{\mathrm{rad}} N. \tag{3}$$

Here, $N = \int dz \Delta n(z)$ denotes the total number of excess electrons within the one-dimensional base. Note that for simplicity Φ, η, N_A, B_{rad}, W, and $N = \int dz \Delta n(z)$ are not written as variables of x and y even though they might vary laterally.

In order to calculate $\Delta n(z)$ for PL-oc and PL-sc, we have to solve the one-dimensional diffusion equation

$$G(z) - \frac{D\Delta n(z)}{L^2} + D\frac{d^2\Delta n(z)}{dz^2} = 0 \tag{4}$$

under steady state illumination. D is the diffusion constant, L is the bulk diffusion length, and $G(z)$ is the generation rate of the excess carriers.

Restricting

$$L_{\alpha,\mathrm{eff}} \ll W \tag{5}$$

it is possible to obtain a simple analytical form for $\Delta n(z)$. Here, $L_{\alpha,\mathrm{eff}} = \cos(\theta_1)/\alpha$ is the effective absorption length. It follows from the absorption coefficient α of the incident monochromatic photon flux j_γ in silicon and the angle θ_1 describing the refraction of j_γ by the front-surface texture. With restriction (5), reflections at the rear surface become negligible and

$$G(z) = \frac{(1-R_f) j_\gamma}{L_{\alpha,\mathrm{eff}}} \exp(-z/L_{\alpha,\mathrm{eff}}) \tag{6}$$

decreases exponentially. With the latter equation, the general solution of Eq. (4) is

$$\Delta n(z) = C\cosh(z/L) - B\sinh(z/L) - A\exp(-z/L_{\alpha,\mathrm{eff}}) \tag{7}$$

and the prefactor A follows

$$A = \frac{(1-R_f) j_\gamma}{D} \cdot \frac{L_{\alpha,\mathrm{eff}}}{1 - L_{\alpha,\mathrm{eff}}^2/L^2}. \tag{8}$$

In order to determine the prefactors B and C, we analyze the impact of the rear surface recombination velocity S_r. For both conditions, PL-oc and PL-sc, the recombination current due to S_r must equal the diffusion current:

$$S_r \Delta n(W) = -D \left.\frac{d\Delta n(z)}{dz}\right|_{z=W}. \tag{9}$$

Due to restriction (5), all terms containing $\exp(-W/L_{\alpha,\mathrm{eff}})$ are neglected in $\Delta n(W)$ and $\Delta n'(W)$, giving a simple relation

$$B = CL/L_{\mathrm{eff}}, \tag{10}$$

between coefficients B and C where

$$L_{\mathrm{eff}} = L\frac{LS_r\sinh(W/L) + D\cosh(W/L)}{LS_r\cosh(W/L) + D\sinh(W/L)} \tag{11}$$

is the effective diffusion length.

For PL-oc no current is extracted at $z=0$ but the impact of the emitter and the front surface has to be taken into account. We lump all losses in the emitter into the emitter saturation current density J_{0e}. The emitter is then treated as a surface acting as a sink for excess carriers with an effective surface recombination velocity S_{eff},[15,16]

$$S_{\mathrm{eff}} = \frac{J_{0e} N_A}{q n_i^2}. \tag{12}$$

The boundary condition at $z=0$ for PL-oc thus follows to

$$S_{\mathrm{eff}} \Delta n_{\mathrm{oc}}(0) = D \left.\frac{d\Delta n_{\mathrm{oc}}(z)}{dz}\right|_{z=0}. \tag{13}$$

With the introduction of the parameter K,

$$K = \frac{1 + S_{\mathrm{eff}} L_{\alpha,\mathrm{eff}}/D}{1 + S_{\mathrm{eff}} L_{\mathrm{eff}}/D}, \tag{14}$$

the boundary condition in Eq. (13) determines $C/A = K L_{\mathrm{eff}}/L_{\alpha,\mathrm{eff}}$ and with Eq. (10) $B/A = KL/L_{\alpha,\mathrm{eff}}$ follows. Consequently, the carrier distribution $\Delta n_{\mathrm{oc}}(z)$ for PL-oc results in

$$\frac{\Delta n_{\mathrm{oc}}(z)}{A} = \frac{KL_{\mathrm{eff}}}{L_{\alpha,\mathrm{eff}}}\frac{\Delta n_d(z)}{\Delta n_d(0)} - \exp(-z/L_{\alpha,\mathrm{eff}}) \tag{15}$$

with the normalized dark carrier distribution

$$\frac{\Delta n_d(z)}{\Delta n_d(0)} = \cosh(z/L) - L/L_{\mathrm{eff}}\sinh(z/L). \tag{16}$$

Note that using restriction (5), Eq. (15) can also be deduced from the more general approach of Duggan and Scott[17] which describes the minority carrier distribution of thin non-

diffused epitaxial layers under optical excitation.

For PL-sc, all excess electrons at $z=0$ are extracted, giving the boundary condition $\Delta n_{sc}(0)=0$. This boundary condition is expressed equally by an infinite emitter saturation current density J_{0e} or an infinite effective surface recombination velocity S_{eff}. Hence, the factor K for PL-sc follows

$$K_{sc} = \lim_{S_{\text{eff}} \to \infty} K = \frac{L_{\alpha,\text{eff}}}{L_{\text{eff}}}. \tag{17}$$

Consequently, for the PL-sc case, the carrier distribution is written as

$$\frac{\Delta n_{sc}(z)}{A} = \frac{\Delta n_d(z)}{\Delta n_d(0)} - \exp(-z/L_{\alpha,\text{eff}}). \tag{18}$$

Finally, as indicated in Eq. (3), we integrate the resulting carrier distributions Δn_{oc} and Δn_{sc}, Eqs. (15) and (18), respectively. Taking into account restriction (5), we obtain for the PL-oc case

$$N_{oc}/A = KL_{\text{eff}}L_C/L_{\alpha,\text{eff}} - L_{\alpha,\text{eff}}, \tag{19}$$

where

$$L_C = L\frac{LS_r[\cosh(W/L) - 1] + D\sinh(W/L)}{LS_r\sinh(W/L) + D\cosh(W/L)}. \tag{20}$$

is the collection length.[18,19] For the PL-sc case, we substitute K in Eq. (19) by K_{sc} of Eq. (17) and end up with

$$N_{sc}/A = L_C - L_{\alpha,\text{eff}}. \tag{21}$$

Finally, the ratio $R=\Phi_{oc}/\Phi_{sc}$ of the measured PL-oc and PL-sc luminescence emission for equal illumination conditions is

$$R = \frac{KL_{\text{eff}}L_C - L_{\alpha,\text{eff}}^2}{L_{\alpha,\text{eff}}L_C - L_{\alpha,\text{eff}}^2}. \tag{22}$$

By an appropriate selection of the excitation wavelength ensuring that

$$L_{\alpha,\text{eff}}^2 \ll KL_{\text{eff}}L_C, \tag{23}$$

$$L_{\alpha,\text{eff}} \ll L_C, \tag{24}$$

$$L_{\alpha,\text{eff}} \ll D/S_{\text{eff}}, \tag{25}$$

we can further simplify our derivation. It allows to neglect $L_{\alpha,\text{eff}}^2$ in the numerator as well as in the denominator of Eq. (22). Applying restriction (25) to Eq. (14), the parameter K simplifies to $(1+S_{\text{eff}}L_{\text{eff}}/D)^{-1}$, thus giving the final result,

$$L_{\text{eff}} \cong L_{\text{eff}}^* = \left(\frac{1}{RL_{\alpha,\text{eff}}} - \frac{S_{\text{eff}}}{D}\right)^{-1}. \tag{26}$$

In the following, L_{eff}^* refers to the effective diffusion length as extracted by Eq. (26), whereas L_{eff} refers to the effective diffusion length obtained by the bulk diffusion length L and the rear surface recombination velocity S_r as indicated in Eq. (11).

In order to ensure the same injection conditions for PL-oc and PL-sc measurements, we reduce the illumination power j_γ for the PL-oc measurement. Since luminescence measurements directly represent the injection conditions [see Eq. (3)], the measured PL-oc photon flux at j_γ^{oc} has to equal the PL-sc photon flux at j_γ^{sc}. Then, for equal photon fluxes, the ratio R follows

$$R = \frac{j_\gamma^{oc}}{j_\gamma^{sc}}. \tag{27}$$

TABLE I. Simulation parameters.

Wafer	300 μm thick, p-type, 1.47 Ω cm
Front	S_f=35825 cm/s, n-type emitter, depth factor =0.001 μm, peak doping=4.2×10^{19} cm^3 (Erfc profile), J_{0_c}=300 fA cm^2, S_{eff}=187 cm/s
Rear	S_r=100 cm/s
Volume	L=300 μm, no injection dependence, electron diffusivity of 28.6 cm^2/s, L_{eff}=298 μm, L_C=189 μm
Optics	No exterior front reflection, planar surface, all internal reflections 100%
Illumination	0.01 W cm^{-2}, 808 nm (L_a=12 μm)

III. SIMULATIONS AND DISCUSSION

To verify that the simplifications due to $L_{\alpha,\text{eff}} \ll W$ are valid, we compare the analytical description of the carrier distribution under oc and sc conditions according to Eqs. (15) and (18), respectively, with carrier distributions obtained by the numerical device simulator PC1D.[20] The parameters used for the simulation are shown in Table I. Carrier losses in the volume of the emitter cannot be described by a specific parameter. Therefore, the emitter is reduced to an ideal thin layer allowing one to directly calculate J_{0e} from the front surface recombination velocity S_f.

In Fig. 1 the two excess carrier distributions Δn_{oc} and Δn_{sc} obtained by PC1D are shown by open symbols. Both

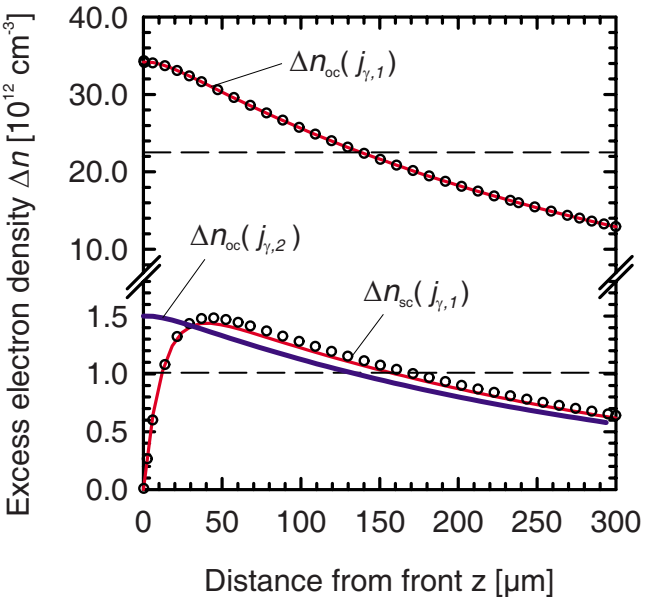

FIG. 1. (Color online) Excess electron densities within the base of a solar cell for PL-oc and PL-sc condition under two different illumination intensities ($j_{\gamma,1}$ and $j_{\gamma,2}$). The solid lines show analytical calculations according to Eqs. (15) and (18). For comparison, the numerical solutions of the device simulation program PC1D are shown as open symbols. The dashed lines indicate the averaged carrier densities. The parameters used for the solar cell simulation are given in Table I.

carrier distributions exhibit the maximum carrier density close to the front surface because the generation of excess carriers mainly occurs within the front region due to the small absorption length of 12 μm. For $z \to 0$, the carrier distribution Δn_{sc} strongly bends down toward zero due to the extraction of the excess carriers at $z=0$. Note that the infinite sink at $z=0$ extracts a vast majority of the generated carriers but not all of them. A small part remains in the base due to the diffusion limitation of the transport.[21] For Δn_{oc}, only a very slight bending is noticed in Fig. 1 for $z \to 0$ as a cause of the emitter saturation current density.

Generated excess carriers at the front region also diffuse toward the rear surface. Due to recombination in the base and at the rear surface, both carrier distributions decrease toward $z \to W$. At $z=W$, the carrier loss due to the rear surface recombination velocity is observable for both carrier distributions by a nonzero slope.

The analytical carrier distributions [see Eqs. (15) and (18)] calculated using the same solar cell parameters (see Table I) are shown in Fig. 1 as solid lines. The qualitative agreement is excellent: the analytical curves lie on top of the simulated curves within the whole base region. The numerical integration of the PC1D carrier distributions compared to the analytical solutions [see Eqs. (19) and (21)] differ for PL-oc by only 0.38% and for PL-sc by 3.31%, giving a good quantitative agreement.

The dashed lines in Fig. 1 represent the average carrier densities $\bar{n}=N/W$ which determine the luminescence emission [see Eq. (3)]. $\bar{n}_{oc}$ has a value of 22.5×10^{12} cm^{-2} and $\bar{n}_{sc}$ of 1.01×10^{12} cm^{-2}. These values demonstrate well the PL-L_{eff} method: $RL_{\alpha,eff}=\Phi_{oc}/\Phi_{sc} \cdot L_{\alpha,eff}$ follows 267 μm from the analytical approach. Considering the impact of the emitter saturation current density as indicated in Eq. (26), the effective diffusion length L^*_{eff} is 317 μm. The effective diffusion length calculated from the parameters L and S_r using Eq. (11) is $L_{eff}=298$ μm, thus PL-L_{eff} slightly overestimates this value by 6.5%.

In order to find the cause of this overestimation, we examine the impact of restrictions (23)–(25) on the determination of L^*_{eff}. Restriction (23), $L_{\alpha,eff} \ll L_{eff} L_C$, and restriction (25), $L_{\alpha,eff} \ll DS_{eff}$, are fulfilled easily by an appropriate selection of the excitation wavelength, whereas restriction (24), $L_{\alpha,eff} \ll L_C$, is more critical. The impact of all three restrictions on L^*_{eff} is shown in Fig. 2 for a 200 μm thick solar cell and an excitation wavelength of 808 nm [$L_{\alpha,eff} \approx 9$ μm for textured (100)-oriented silicon]. Since L_{eff}, L^*_{eff}, and L_C are functions of L and S_r, a parameter space is obtained. It demonstrates that, in general, L^*_{eff} will overestimate the real L_{eff} slightly, with a better accuracy for larger L_{eff} values. For L_{eff} values larger than 155 μm, the deviation of L^*_{eff} is below 10%.

Figure 1 also demonstrates the approach to maintain the same injection densities, as indicated by Eq. (27). The blue line [marked with $\Delta n_{oc}(j_{\gamma,2})$] shows the PL-oc carrier distribution under reduced illumination power resulting in the same average injection condition for the sc and the oc case.

As explained for the exemplary calculated carrier distributions in Fig. 1, the impact of the emitter saturation current density is not negligible. For a quantification of this impact,

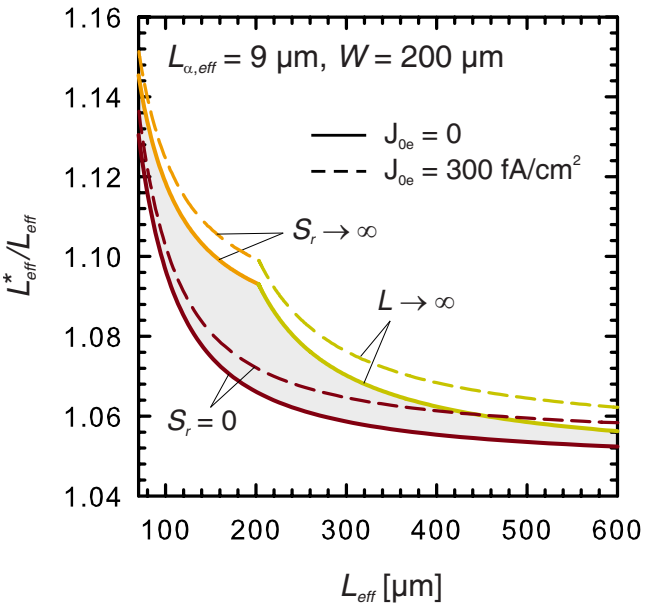

FIG. 2. (Color online) Simulated parameter space of the deviation of L^*_{eff} to L_{eff} for two J_{0e} values. L^*_{eff} was extracted from the ratio of the PL-oc and the PL-sc signals as indicated by Eq. (26) and L_{eff} was calculated from L and S_r according to Eq. (11).

we calculate the ratio of the open circuit and short circuit luminescence signals for different J_{0e} values using the same parameters as before (see Table I). Note that for this calculation not only J_{0e} is important but also the base doping N_A, as indicated in Eq. (12). The results are shown in Fig. 3 as lines (solid line: 200 fA/cm^2, dashed line: 400 fA/cm^2, and dotted line: 800 fA/cm^2). For the J_{0e} values shown in Fig. 3, the impact of the emitter is negligible for L_{eff} values shorter than 250 μm but becomes dominant for values larger than 400 μm. For the latter case, PL-L_{eff} is only applicable if J_{0e}

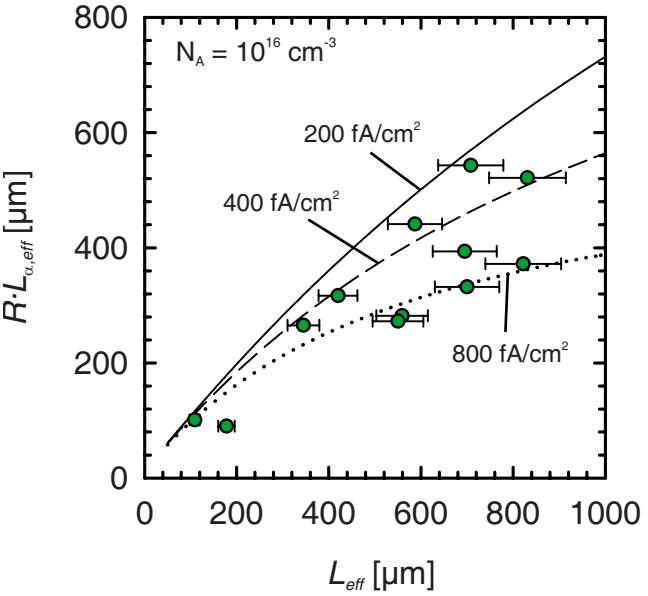

FIG. 3. (Color online) Solid lines: simulation of $RL_{\alpha,eff}$ for different J_{0e} values ($N_A=10^{16}$ cm^{-3}). Circles: measured data set with L_{eff} values obtained from PL-L_{eff} and quantum efficiency analysis for different solar cells. For PL-L_{eff} no assumptions about the emitter were made, thus $RL_{\alpha,eff}$ is plotted instead of L^*_{eff}.

is known accurately or if it can be assumed to be small. This might appear as a disadvantage at first glance. However it allows a nondestructive determination of J_{0e} of solar cells. The only requirement is a precise knowledge on L_{eff}, which, for example, can be determined using quantum efficiency analysis.

IV. EXPERIMENTAL SETUP

We demonstrate the applicability of PL-L_{eff} using a spectral response and a PL setup. Here, we only introduce the PL setup since the details of the used spectral response setup were already published elsewhere.[22]

The PL setup comprises of a laser to stimulate the generation of luminescence photons, a bipolar power source connected to the solar cell, and an indium gallium arsenide sensor to measure the luminescence emission.

The used gallium arsenide (GaAs) diode laser exhibits a central wavelength of 809 nm having an absorption length of $\sim 12\ \mu$m in silicon. A beam homogenizer based on microlenses shapes the fiber output beam. The whole solar cell area is illuminated with an homogeneity of $\pm 10\%$. The maximal continuous wave output power of the laser is 30 W. Considering the losses of the fiber and the optics, a $15.6 \times 15.6\ \mathrm{cm}^2$ solar cell can be illuminated by a power equivalent of up to 1 sun.

The solar cell is mounted on a vacuum chuck and contacted by a number of spring-loaded contact pins on each busbar. A four quadrant source controls the applied voltage using a four-point contacting scheme. For PL-oc conditions no current is extracted, whereas for PL-sc conditions, the solar cell is hold at zero voltage. During the measurements the chuck is temperature controlled by a closed-loop water chiller.

We use an indium gallium arsenide (InGaAs) detector for the measurement of the luminescence emission. The detector is sensitive to photons ranging from 900 to 1700 nm and collects photons from a $2 \times 2\ \mathrm{cm}^2$ area.

For the measurements, we have to account for several experimental difficulties. Firstly, the beam homogenizer, the solar cell, and the InGaAs detector are mounted in a dark box to guard against the interference of stray light. Secondly, we subtract the dark signal of the detector which we obtain by a measurement with equal exposure time but without any stimulation of luminescence. Thirdly, the reflected laser light at the solar cell surface is blocked using two optical filters. The first one, a bandpass filter with a high optical density for wavelengths of >820 nm is mounted after the homogenizer. This filter blocks the emission of the laser at the low energy side since the sharp laser line is weakly superimposed by a broad spectrum of spontaneous emission of the GaAs laser diode. The second filter, a 1000 nm longpass filter, is mounted in front of the camera. This filter blocks the directly reflected laser light but exhibits a high transmission for the luminescence photons. Simulations show that this longpass filter is sufficient to neglect the reabsorption in Eq. (3) due to the distribution of the luminescence spectra in combination with the high sensitivity of the InGaAs detector for wavelengths up to 1700 nm.

V. MEASUREMENTS AND DISCUSSION

In order to demonstrate the PL-L_{eff} approach experimentally, we compare resulting L_{eff} values to values obtained from quantum efficiency analysis (IQE).[1] We investigate 12 mono- and multicrystalline industrial screen-printed solar cells with sizes of 125×125 and $156 \times 156\ \mathrm{mm}^2$ from different suppliers.

For an accurate comparison of the two methods, identical injection levels are essential. For PL-L_{eff}, the injection level is determined from the extracted short circuit current $I_{\mathrm{sc}}^{\mathrm{PL}}$ of the PL-sc measurement. Note that for the PL-oc measurement, the excitation power is reduced until the same luminescence signal is measured as in the PL-sc case. For the quantum efficiency analysis, the injection level is usually determined by the extracted short circuit current $I_{\mathrm{sc}}^{\mathrm{QE}}$. However, the current $I_{\mathrm{sc}}^{\mathrm{QE}}$ is not directly comparable with $I_{\mathrm{sc}}^{\mathrm{PL}}$ since bias light assisted QE measurements determine the differential quantum efficiency.[23] Our approach is to measure the differential EQE bias ramp at a certain wavelength (1000 nm). By integrating these differential EQE values, the corresponding injection level of the absolute measurement can be calculated.[24]

The results of this comparison are shown in Fig. 3, where for the PL-L_{eff} analysis no assumptions about the emitter were made, thus only $R\ L_{\alpha,\mathrm{eff}}$ is shown. From Fig. 3 we see that all PL-L_{eff} values lie in the same range as the SR-L_{eff} values but underestimate them for SR-L_{eff} $>400\ \mu$m.

We explain this underestimation by the impact of the emitter saturation current, as shown in Fig. 3 by solid lines. Compared to the calculated curves, all measured data points lie in the expected range of realistic J_{0e} values. Even though we carefully intended to measure the solar cells for PL-L_{eff} and QE at the same position and the same injection level, deviations in these parameters cannot be totally excluded.

VI. SUMMARY AND OUTLOOK

We derived an analytical description of the PL-oc and the PL-sc luminescence emissions of a standard solar cell. We further demonstrated that the ratio of two luminescence measurements obtained under open circuit and short circuit condition yields the effective diffusion length. This PL-based determination of the effective diffusion length was successfully applied to various solar cells. The comparison to values obtained by the analysis of IQE data shows a good agreement. For large L_{eff} values, it is important to take the impact of the emitter into account, thus PL-L_{eff} can be used to determine J_{0e} by a prior measurement of L_{eff}. The PL-L_{eff} approach is quick and simple; no calibration or detailed information on the setup is necessary since optical properties of the setup cancel out completely.

For the presented method, only the current loss in the emitter was included, recombinations at shunts and in the space charge region were neglected. Device simulations using PC1D show that shunts of $>1000\ \Omega\ \mathrm{cm}^2$ have a negligible impact on the determined L_{eff}.

In general, PL-L_{eff} is applicable to spot as well as to spatially resolved measurements using a camera. For spa-

tially resolved measurements, the impact of balancing currents due to the grid and the emitter have to be regarded in PL-oc. We therefore expect the resulting images to suffer from a lower contrast compared to mappings obtained by SR-LBIC or by the method introduced by Würfel *et al.*[8]

ACKNOWLEDGMENTS

The authors would like to thank Bernhard Fischer for fruitful discussions. Many thanks go to Martin Wolf for carrying out spectral response measurements. This work was funded by the Federal Ministry for the Environment, Nature Conservation and Nuclear Safety under Contract No. 0327661.

[1]P. Basore, *Proceedings of the 23rd Photovoltaic Specialists Conference*, Louisville, KY (IEEE, New York, 1993), pp. 147–152.
[2]W. Warta, J. Sutter, B. Wagner, and R. Schindler, *Proceedings of the Second World Conference and Exhibition on Photovoltaic Solar Energy Conversion*, Vienna, Austria (EC Joint Research Center, Ispra, 1998), pp. 1650–1653.
[3]K. Taretto, U. Rau, and J. Werner, J. Appl. Phys. **93**, 5447 (2003).
[4]J. Haynes and H. Briggs, Phys. Rev. **86**, 647 (1952).
[5]W. Michaelis and M. Pilkuhn, Phys. Status Solidi **36**, 311 (1969).
[6]K. Schick, E. Daub, S. Finkbeiner, and P. Würfel, Appl. Phys. A: Solids Surf. **54**, 109 (1992).
[7]T. Fuyuki, H. Kondo, T. Yamazaki, Y. Takahashi, and Y. Uraoka, Appl. Phys. Lett. **86**, 262108 (2005).
[8]P. Würfel, T. Trupke, T. Puzzer, E. Schäffer, W. Warta, and S. Glunz, J. Appl. Phys. **101**, 123110 (2007).
[9]T. Kirchartz, A. Helbig, and U. Rau, Sol. Energy Mater. Sol. Cells **92**, 1621 (2008).
[10]U. Rau, Phys. Rev. B **76**, 025303 (2007).
[11]T. Trupke and R. Bardos, *Proceedings of the 31st Photovoltaic Specialists Conference*, Lake Buena Vista, FL (IEEE, New York, 2005), pp. 903–906.
[12]T. Trupke, J. Appl. Phys. **100**, 063531 (2006).
[13]K. Bothe, P. Pohl, J. Schmidt, T. Weber, P. Altermatt, B. Fischer, and R. Brendel, *Proceedings of the 21st European Photovoltaic Solar Energy Conference*, Dresden, Germany (WIP, Munich, 2006), pp. 597–600.
[14]P. Altermatt, F. Geelhaar, T. Trupke, X. Dai, A. Neisser, and E. Daub, Appl. Phys. Lett. **88**, 261901 (2006).
[15]D. Kane and R. Swanson, *Proceedings of the 18th Photovoltaic Specialist Conference*, Las Vegas, NV (IEEE, New York, 1985), pp. 578–583.
[16]A. Cuevas, Sol. Energy Mater. Sol. Cells **57**, 277 (1999).
[17]R. Duggan and G. Scott, J. Appl. Phys. **52**, 407 (1981).
[18]R. Brendel and U. Rau, Solid State Phenom. **67**, 81 (1999).
[19]K. Bothe, D. Hinken, K. Ramspeck, B. Fischer, and R. Brendel, *Proceedings of the 22nd European Photovoltaic Solar Energy Conference*, Milan, Italy (WIP, Munich, 2007), pp. 1673–1677.
[20]D. Clugston and P. Basore, *Proceedings of the 26th Photovoltaic Specialists Conference*, Anaheim, CA (IEEE, New York, 1997), pp. 207–210.
[21]T. Trupke, E. Pink, R. Bardos, and M. Abbott, Appl. Phys. Lett. **90**, 093506 (2007).
[22]B. Fischer, Ph.D. thesis, University of Konstanz, 2003.
[23]J. Metzdorf, Appl. Opt. **26**, 1701 (1987).
[24]B. Fischer, M. Keil, P. Fath, and E. Bucher, *Proceedings of the 29th Photovoltaic Specialists Conference*, New Orleans, LA (IEEE, New York, 2002), pp. 454–457.